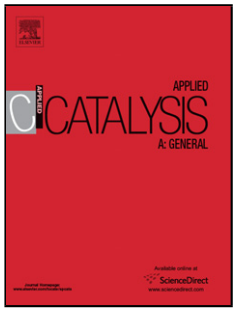

Title: Development and Testing of an Additively Manufactured Monolithic Catalyst Bed for HTP Thruster Applications

Author: K. Essa H. Hassanin M.M. Attallah N.J. Adkins A.J. Musker G.T. Roberts N. Tenev M. Smith

PII: S0926-860X(17)30217-X
DOI: http://dx.doi.org/doi:10.1016/j.apcata.2017.05.019
Reference: APCATA 16241

To appear in: *Applied Catalysis A: General*

Received date: 20-2-2017
Revised date: 18-5-2017
Accepted date: 19-5-2017

Please cite this article as: K. Essa, H. Hassanin, M.M. Attallah, N.J. Adkins, A.J. Musker, G.T. Roberts, N. Tenev, M. Smith, Development and Testing of an Additively Manufactured Monolithic Catalyst Bed for HTP Thruster Applications, *Applied Catalysis A, General* (2017), http://dx.doi.org/10.1016/j.apcata.2017.05.019

Development and Testing of an Additively Manufactured Monolithic Catalyst Bed for HTP Thruster Applications

K. Essa[(1)], H. Hassanin[(2,3)], M.M. Attallah[(3)], N.J. Adkins[(3)], A.J. Musker[(4)], G.T. Roberts[(5)], N.Tenev[(5)], M. Smith[(6)]

[(1)]School of Mechanical Engineering, University of Birmingham, UK, Email: k.e.a.essa@bham.ac.uk
[(2)]School of Mechanical and Aerospace Engineering, Kingston University, Email: h.hassanin@kingston.ac.uk.
[(3)] School of Metallurgy & Materials, University of Birmingham, UK
[(4)]DELTACAT Ltd and University of Southampton, UK, Email: tony.musker@deltacatuk.com
[(5)]Aerodynamics & Flight Mechanics Research Group, University of Southampton, UK, Email: gtr@soton.ac.uk
[(6)]TEC-MPC, ESA/ESTEC, NL, Email: Matthew.Smith@esa.int

Keywords: additive manufacturing, 3-D printing, selective laser melting, hydrogen peroxide catalysis, green space propulsion

Abstract

Additive manufacturing (AM), also known as 3D printing, is a revolutionary manufacturing technology that has attracted many industries in the past two decades. This is because AM enables the manufacturing of complex-shaped geometries without the limitations of other manufacturing techniques. In this paper, the design, development and testing of additively manufactured, monolithic catalyst beds are described. A novel design methodology was employed and achieved catalyst bed designs with complex geometry and high geometrical surface area whilst achieving an acceptable pressure drop. Catalyst bed samples incorporating alumina ceramic lattices with strut diameters ranging from 0.15 to 0.30 mm were fabricated via AM and a subsequent heat treatment. The surface areas of the samples were improved using different wash coats, including the use of gamma alumina and a mixture of gamma alumina and carbon nanotubes (CNT). Manganese oxides were used to coat the catalyst bed and decompose hydrogen peroxide. Four full-scale catalyst beds with the most promising candidate geometries and wash coats were then manufactured and subsequently tested in a 20 N-class HTP (High Test Peroxide) monopropellant thruster. The firing results show that the additively manufactured catalyst beds generally outperformed the baseline catalyst bed containing ceria pellets that were also coated with manganese oxides.

1. Introduction

Hydrazine and its derivatives, such as monomethylhydrazine (MMH) and unsymmetrical dimethylhydrazine (UDMH), are the most commonly used propellants for the propulsion and control of a wide range of spacecraft and satellites. They have been the most favourable choice for aerospace applications for more than 50 years as they show excellent flight performance. However, they are highly toxic and carcinogenic. The use of these substances carries with it the burden of enhanced health and safety protection for working personnel [1, 2]. Recently, low toxicity ('green') storable liquid propellants have attracted a considerable amount of attention as replacements for hydrazine based propellants. The movement towards the use of green propellants is not only being driven by concerns regarding the toxicity of hydrazine and its derivatives, but more importantly by the possibility of these chemicals being banned [3, 4]. Hydrogen peroxide (H_2O_2) is a popular substance used in many industrial applications such as food processing, cosmetics, and wastewater treatment [5, 6]. High-test peroxide (HTP) is a highly concentrated solution of hydrogen peroxide, with a concentration range from 85 % to 98 %. HTP is considered to be a 'green' propellant because it only exhausts oxygen and water upon catalytic or thermal decomposition. It is particularly attractive because of its high density and low cost. HTP also promises considerable cost savings due to simplifications in health and safety procedures during production, storage and handling [7-9].

For an HTP thruster to work effectively the HTP must be decomposed catalytically to produce superheated steam and oxygen, which can then be used either as the exhaust stream in a monopropellant application, or as the oxidiser in a bi-propellant application. In both applications, the thruster performance relies critically on the

ability of the catalyst bed to decompose fully the HTP. The bed must be capable of rapid and repeatable performance over the many operational cycles imposed by typical mission profiles. A high-performing catalyst bed will offer a high surface area (per unit volume of bed) and a low pressure drop, although these two requirements are typically in conflict [10-12].

HTP catalyst beds often incorporate either metallic gauzes or screens (typically pure silver, or silver-plated), or ceramic pellets coated with an active catalytic phase which could be metallic or some type of metal oxide [13, 14]. To achieve the required surface area per unit volume, the metal screens must by tightly-packed and therefore usually exhibit relatively high pressure drops. Pellet-based beds usually have higher surface areas and rather lower pressure drops, but the relative movement of the pellets, caused by the vigorous decomposition of the peroxide, can cause fragmentation and loss of pellets from the bed, possibly resulting in reduced lifetime [15, 16]. An alternative to both the above types is a monolithic bed, which is conventionally manufactured by extrusion of a ceramic paste through a die and then coated with an active phase. However, the flow path for the propellant is through straight channels which offer relatively low surface area so such beds are prone to a phenomenon known as “flooding”, which quenches the decomposition reaction [17]. To prevent this, the bed loading (mass flow rate of propellant per unit cross-sectional area) must either be kept very low, or the beds are made very long. This leads to catalyst beds that are relatively large compared with beds that incorporate pellets or metal screens, with attendant heat loss issues.

Additive manufacturing (AM) is a disruptive technology that is developing rapidly. It promises to find widespread applications, especially in the aerospace industry. Compared with conventional manufacturing techniques, the major benefits of AM are

product design customisation for functionality, with reduced material wastage and low energy usage, and reduced lead-time. However, perhaps the greatest benefit of all is that AM enables design innovation, allowing the production of parts with complex geometry that would be impossible to manufacture by conventional means [18-21].

For these reasons, the European Space Agency (ESA) initiated a recent research and development activity with the goal of enhancing HTP catalyst bed design through the use of AM. A monolithic catalyst bed with a complex internal geometry produced by AM could in principle overcome the limitations of the former types of beds described earlier and is the subject of the study described in this paper. Here, we describe the design and development of monolithic catalyst beds that are manufactured using AM and tested in a relatively small (20 N class) monopropellant thruster employing HTP. Computer Aided Design (CAD) and Computational Fluid Dynamics (CFD) were employed for the optimisation of the catalyst bed geometry. Alumina catalyst beds were fabricated using selective laser melting (SLM) and subsequently coated using a manganese oxide catalytic layer. The performance of the catalyst beds was initially evaluated by carrying out simple qualitative and semi-quantitative tests on a range of small scale samples and then, after down-selection, thruster firing tests on full-scale beds.

2. Design and Experimental

2.1 20 N Thruster Design

The University of Southampton had previously successfully tested a monopropellant thruster which had been designed to produce 20 N at sea-level conditions with 87.5 % concentration HTP at a propellant mass flow rate of 17.7 g/s [16]. In that previous work the catalyst bed chamber contained either ceramic pellets or metallic gauzes as the catalyst material; a monolithic catalyst bed was not investigated at that time. For this current work, as the baseline comparator for the AM monolithic catalyst beds that were developed, it was decided to use pellets of cerium oxide (ceria) which had been impregnated with a catalytic active phase comprising oxides of manganese (MnO_x). Previous work [22] carried out at the University of Southampton, in which a variety of potential catalyst types was investigated, had indicated that these MnO_x-coated pellets exhibited a good reactivity and, of those catalysts tested in the 20 N thruster, provided the best level of performance [16]. Hence if the AM-fabricated monolithic catalyst bed exhibited a performance that was as good as, or exceeded, that of the ceria pellets when tested in the thruster, this would be considered a very promising development [23].

In the current research, it was decided to retain the same geometry of catalyst bed chamber as in the previous work, with only slight design modifications required to allow two monolithic catalyst support elements to be inserted into the catalyst bed chamber, see Figure 1 in which the propellant flow is from right to left. The latter incorporated a baffle at approximately the mid-point, designed to prevent the preferential flow of undecomposed liquid HTP along the interior wall of the bed

chamber, a phenomenon known as channelling. One of the catalyst supports slid in upstream of the baffle and the other downstream.

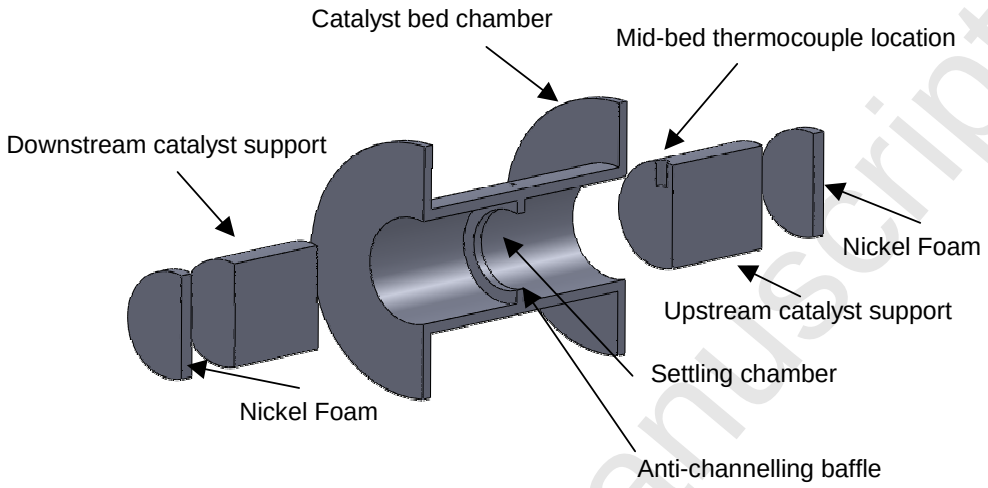

Figure 1: An exploded view of the catalyst bed chamber assembly

Provision was made to allow access for a thermocouple probe just upstream of the baffle to measure the temperature of the HTP decomposition products at approximately the mid-bed location. The nominal outer diameter of the catalyst bed supports was 21 mm and each was approximately 24 mm long.

Nickel foam discs were placed at the upstream and downstream ends of the bed to accommodate any compressive forces transmitted to the bed and hence prevent damage when the bed was connected to the remainder of the thruster components (see Figure 1). The latter included, upstream of the catalyst bed chamber, a showerhead-type injector plate with a plenum chamber upstream which enabled the pressure and temperature of the incoming HTP to be measured.

Downstream of the bed chamber, a convergent-divergent nozzle assembly was attached. The nozzle served to pressurise the catalyst bed and was designed to

expand the decomposition products to sea-level atmospheric conditions at the thruster exit when operating at a pressure of 12 bar absolute. Such a nozzle will give the optimum thruster performance. Had the nozzle been designed for vacuum operation (as in the space environment) it would have had a higher expansion ratio (ratio of exit to nozzle throat areas) and the thrust produced would have been higher. The nozzle assembly also incorporated a plenum chamber which allowed the pressure and temperature of the HTP decomposition products at the bed exit to be measured.

Between the bed exit and the nozzle assembly was a porous catalyst retainer plate. Although strictly speaking this component was not necessary with the monolithic beds, it was left in place so that the thermal mass of the metal components of the thruster assembly remained the same as that when tested with the ceramic pellet catalyst bed used as a baseline comparator. It should be noted that the thruster assembly has been used for catalyst testing only and so has not been optimised from a thermomechanical point of view.

An exploded view of the original thruster components is shown in Figure 2.

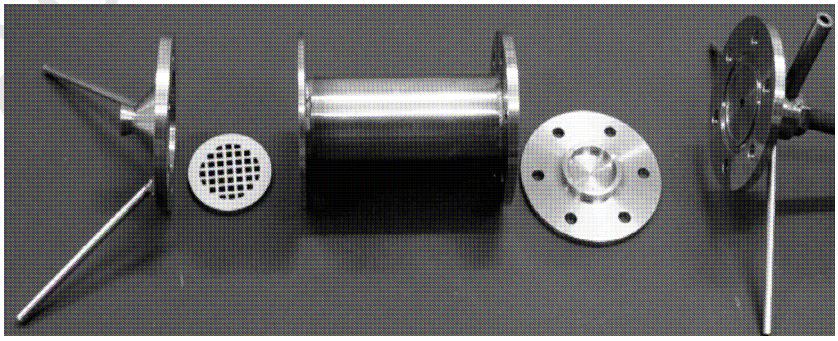

Figure 2: Original thruster components

From right to left these are: the HTP injector plenum (with pressure transducer and thermocouple standpipes attached); the showerhead-type injector plate; the catalyst bed chamber; the catalyst retainer plate and finally the nozzle assembly, also with pressure transducer and thermocouple standpipes attached.

The thruster was mounted to a swing-arm thrust stand. This, and the nitrogen-pressurised propellant delivery system (PDS), is identical to that described in [24, 25]. The PDS included a turbine flow meter which provided a measurement of the propellant mass flow rate. Although the thrust produced was measured, the main emphasis of the thruster performance evaluation was based on the characteristic velocity, C^*, since this is one of the main parameters that describe the performance of the catalyst bed, the other being the catalyst bed pressure drop. In this work the overall pressure drop across the catalyst bed and injector plate was determined from the pressure measurements that were taken. Knowing the propellant mass flow rate and the injector plate flow characteristics, the pressure drop across the catalyst bed alone could then be estimated.

For a given monopropellant there is a theoretical maximum value of C^*, which is obtained when the propellant is fully decomposed (or reacted) under isentropic conditions. Often, as here, the performance of the catalyst bed is assessed by estimating the C^* efficiency, which is the actual value of C^* estimated from experimental measurements, divided by the theoretical maximum value. A well-performing catalyst bed will exhibit a C^* efficiency in excess of 90 %.

In this work, two values of C^* were estimated, one based on the temperature recorded at the centre-line in the nozzle plenum chamber (equation (1)) and the

other based on the measured nozzle plenum chamber pressure and propellant flow rate, equation (2).

$$C^* = \sqrt{\frac{1}{\gamma}\left(\frac{\gamma+1}{2}\right)^{\frac{\gamma+1}{\gamma-1}} \frac{R_u T_c}{\bar{M}}} \quad (1)$$

$$C^* = \frac{P_c A_t}{\dot{m}} \quad (2)$$

In the above, T_c and P_c are the measured nozzle plenum temperature and pressure, A_t is the nozzle throat area, $\dot{m}$ is the propellant mass flow rate, R_u is the universal gas constant, $\bar{M}$ is the average molar mass of the decomposition products and γ is the ratio of specific heats. If the thruster operates under ideal (isentropic) conditions, the two values would be identical. Because of non-idealities in the thruster operation and errors in the measured quantities, in practice the two usually differ by a small amount.

2.2 Catalyst Bed Design

As described earlier, one of the key design requirements for the catalyst bed is that it should have a large surface area per unit volume. Additive manufacturing offers the possibility of developing a catalyst bed with a complex internal geometry, and consequently tortuous flow path, which naturally increases the bed surface area and the residence time of the propellant within the bed, both of which promote HTP decomposition. However, in so doing the pressure drop across the bed would be increased and so a design trade-off is necessary.

One of the main limitations of additive manufacturing is the overhang features, which requires building them on loose powder. This can lead to distortions and the failure

of the build. The exception of this limitation is to use self-supporting structures. The overhang angle of self-supporting structures depends on the material and the process parameters but in most cases, it is about 45 °.

Nodally-connected diamond lattice structures were selected since these would be self-supporting, satisfying AM limitations, and would create a structure that is strong and has the required tortuous flow path [25-27]. Nodally-connected diamond lattice structures have a wide range of applications, such as in biomedical implants, shock or vibration damping and acoustic absorption [28-31]. Figure 3(a) shows an example of a nodally-connected diamond lattice structure and its unit cell. It is clear that the lattice geometry in terms of strut dimensions and arrangement influences the surface area presented to the propellant and the pressure drop experienced by the bed. Hence, a trade-off study is necessary to attempt to identify the optimum geometric characteristics of the monolithic bed, given the dimensional constraints imposed by the thruster. In order to carry out the trade-off study, four different lattice designs with various strut dimensions and arrangement were created using a CAD model, and these were then imported into a CFD package to estimate the pressure drop across the bed. The objective here is to obtain a design with the highest geometrical surface area and an acceptable pressure drop.

Figure 3(b) – 3(d) shows the four different nodally-connected diamond shapes that were designed; designs 1 and 2 were similar in geometry but had different strut lengths (2 mm and 1 mm, respectively). In design 3, the lattice struts have been arranged in hexagonal shape. Finally, in design 4, the struts have been arranged so that one layer of lattice structure is rotated by 90 ° from the previous layer to allow a maximum interaction between the propellant and the catalyst bed.

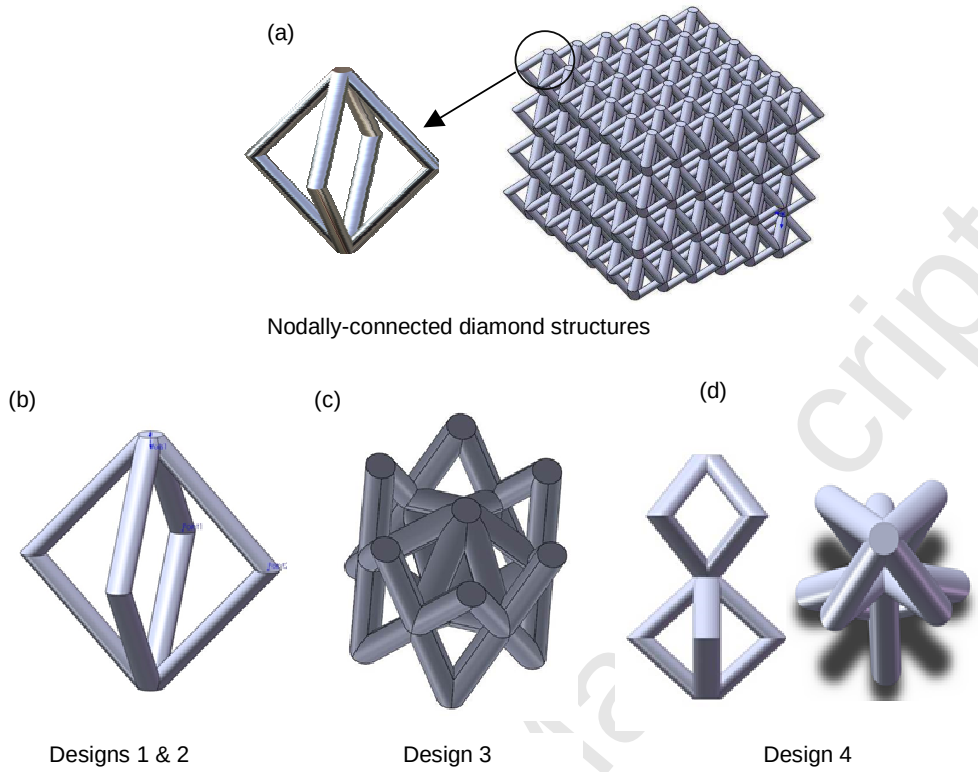

Figure 3: The Nodally-connected diamond structures used in this study

The aforementioned designs were used in developing the catalyst bed models. Figure 4 is an example of one of the full 3-D catalyst bed designs that were imported into the CFD package within the SolidWorks simulation toolbox. Each unit cell was arrayed in XYZ directions to form the catalyst bed support, and the thruster bed chamber dimensions were reproduced. The boundary conditions applied were 17.7 g/s mass flow rate and 12 bar pressure at the exit of the catalyst bed. The catalyst bed support was modelled using solid elements. Only the gas phase (steam) has been considered in the CFD model, which was used to predict the pressure drop across the bed and the velocity within the bed. Additionally, the geometrical area and the pressure drop of each catalyst bed design were calculated. It is recognised that a single-phase, non-reacting CFD model would not fully represent the processes

taking place in the bed but it was felt that, for design comparisons, this relatively simple CFD model would be adequate.

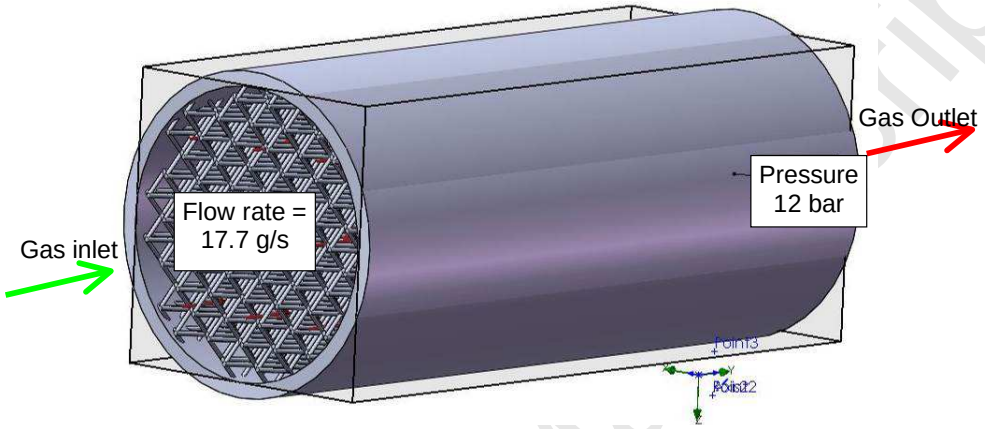

Figure 4: One example of the full 3D CAD model with boundary conditions

2.3 Manufacturing

The catalyst bed material was chosen to be alumina, since this material exhibits advantageous high temperature mechanical and thermal properties. Selective laser melting (SLM) was the AM technology that was used to fabricate the proposed alumina catalyst bed. LPW Technology Ltd supplied the AlSi10Mg powder as the feedstock for the bed structure. A Concept Laser M2 SLM system, with a Nd:YAG laser of a wavelength of 1075 nm, a constant beam spot size of 50 μm in diameter, a maximum laser output power of 400 W and a maximum laser scanning speed of 4000 mm/s, was used to build lattice structures. The powder was sieved using 65 μm mesh size. The average size of the powder is 22.8 μm and the Hausner ratio is 1.18 (<1.25), which means the flow-ability of the powder is good. Alumina lattice

structures with strut diameters between 0.15 and 0.30 mm were successfully achieved using the method described in the literature [32] which is based on the heat treatment of AlSi10Mg lattice structures at 1600 ºC.

A number of alumina cubic samples with dimensions of about 6x6x6 mm were produced for reactivity evaluation purposes. Initially, alumina samples with all the four lattice designs described above were manufactured. One of the key design requirements for catalyst bed was for the bed to have a large surface area per unit volume. Therefore, wash coat processes were used to promote the surface quality of the AM samples. In particular, a gamma alumina wash coat and a mixture of gamma alumina and carbon nanotubes (CNT) were used in the experiment.

In the preparation of the gamma alumina wash coat, D-3005, a ceramic dispersant supplied by Rohm and Haas comprising an ammonium salt of a polyelectrolyte, was added to deionised water and mixed with the aid of magnetic stirrer for 5 min. Next, alumina powder supplied by Sigma Aldrich, comprising 50% gamma alumina (mean particle size 50 nm) and 50% alpha alumina (mean particle size 1 µm), was added to the mixture to achieve a constant solid loading of 5 % vol. The de-agglomeration of the powder was achieved by mechanical stirring for 1 h followed by ultrasonic processing for 10 min. Afterwards, acrylic-based binders B-1000 and B-1007, also supplied by Rohm and Haas, were added at a ratio of 1:4 and mixed for 30 min using a low speed stirrer to reduce any foaming. Next, the additive-manufactured alumina lattices were immersed in the prepared solution and placed inside a vacuum chamber at 0.3 bar to ensure that the solution penetrated inside all the lattice spaces. The samples were then dried in a Petri dish and heated to 750 °C for 2 h.

In the preparation of the CNT wash coat, sodium dodecyl sulphate was added to deionised water and mixed with the aid of magnetic stirrer for 5 min. Multi-walled carbon nanotubes (MWCNTs) were supplied by Alfa Aesar (Outer diameter of 20-30 nm, purity > 95%) was added to the solution with a mass ratio of 1:10 and agitated in an ultrasonic cleaner for 1 h. This mixture was then added either to the sodium permanganate monohydrate active phase solution (see below) or to the gamma alumina wash coat solution, prepared as described above.

It is well-known that manganese oxides (here referred to generically as MnO_x) have very strong catalytic capabilities to decompose HTP [22]. A stable layer of MnO_x on alumina can be obtained upon impregnation with a suitable precursor solution and subsequent calcination [33]. In this work, the AM alumina samples were impregnated with a sodium permanganate monohydrate precursor solution. Firstly, the samples were heated before impregnation to 500 °C for 2 h to remove any adsorbed moisture and then allowed to cool. Meanwhile, sodium permanganate monohydrate crystals and distilled water were mixed at a ratio of 3:5 and agitated using a magnetic stirrer at 60 °C, for 1 h. Once cool, the samples were then placed in the solution and stirred for 2 h. Next, the samples were removed and placed in a furnace and heated at 90 °C for 1 h to dry them and then to 800 °C for a further 2 h for calcination to take place.

2.4 Drop and dynamic weighing tests

An initial batch of 15 test samples was manufactured and then evaluated firstly by carrying out simple, qualitative tests with HTP (so-called “drop tests”). The aim of these initial tests was to identify those samples which appeared to offer good reactivity and were thermo-mechanically robust. For this initial evaluation, samples

with different strut diameters (0.15 to 0.30 mm), strut lengths (0.75 to 2.0 mm), and wash coat processes were tested. At this stage the lattice design was confined to the simple diamond-shaped structure (designs 1 and 2 in Figure 3). Table 1 describes the details of the samples prepared.

Table 1: AM samples prepared for initial evaluation

Sample number	Strut length, diameter (mm)	Wash coat	Active phase
0	2, 0.3	None	None
1A	0.75, 0.15	None	MnOx
2A	1.5, 0.15	None	MnOx
3A	1.5, 0.15	alumina	MnOx+CNT
4A	2, 0.15	None	MnOx
5A	2, 0.3	alumina+CNT	MnOx
6A	1.5, 0.3	None	MnOx twice
7A	2, 0.3	None	MnOx
8A	1.5, 0.15	None	MnOx,CNT
9A	2, 0.3	None	MnOx,CNT
10A	1.5, 0.15	None	MnOx
11A	1, 0.3	None	MnOx
12A	1, 0.15	alumina	MnOx twice
13A	2, 0.3	alumina	MnOx
14A	1, 0.3	alumina+CNT	MnOx

Sample 0 had no wash coat or active phase coating and was used to confirm that the alumina substrate was inert to HTP. The “A” designates alumina as the lattice base material. As noted earlier, in some cases (samples 3A, 8A, 9A) the CNT solution was added to the active phase (MnO_x) solution whereas in others (samples 5A, 14A) the CNT solution was added to the gamma alumina wash coat solution. Two samples (6A, 12A) had a double coating of the active phase solution to create a thicker layer of the active phase on the lattice support.

The tests involved exposing the samples to a few drops of 87.5 % concentration hydrogen peroxide (HTP), supplied by Evonik Industries AG, and simply observing and noting the vigour of the decomposition reaction that took place, using a

qualitative scale for comparison. The drop tests were repeated for each sample in order to observe whether or not the reactivity had declined at all after the first tests had taken place. If so, this might give an indication of a limited lifetime of the catalyst sample.

A series of dynamic weighing tests – which were more quantitative in nature – were then conducted with the down-selected samples that had appeared to be most reactive in the drop tests. These tests were aimed at measuring and comparing the reactivity of the samples after repeated immersions in HTP. The method involved immersing each of the samples in 10 g of HTP (65 % concentration) in a beaker and measuring the loss of mass as oxygen and steam is evolved from the decomposing HTP. The rate at which the mass is lost gives an indication of the reactivity of the sample: a sample that gives a higher rate of mass loss is considered to be more reactive. The tests were conducted with a lower concentration of HTP than the initial drop tests because it was considered to be unsafe to do otherwise. A measurement of the HTP liquid temperature was also taken simultaneously: the peak temperature was achieved when the HTP solution started to boil (at about 105 °C for 65 % HTP at ambient pressure). The initial rate of change of temperature gives another indication of the sample's reactivity. Each test lasted until 90 % of HTP was consumed, or the mass of the system was no longer changing, whichever was the sooner. If neither of these conditions was reached after 600 s the test was stopped. The tests were repeated with the same sample 5 times, from which the response with each immersion can be compared to gauge the decay in reactivity. This gives an indication of the possible useful lifetime of the catalyst material although, of course, it is not properly replicating the conditions the catalyst would experience

within a thruster. The performance of the samples was compared with those of a similar volume of MnO_x-coated ceria pellets.

2.5 Thruster test strategy

Thruster tests were carried out with full-scale catalyst beds, having previously identified the most promising internal geometries and wash-coat/active phase coatings from the initial evaluation tests. The thruster test strategy adopted for this project was constrained by the available amount of 87.5 % peroxide. This was important when planning the test runs because to achieve the design peroxide mass flow rate of 17.7 g/s the gas delivery pressure had to be set very accurately. Because of the thermal capacity of the over-engineered thruster, the run parameters, such as chamber pressure and decomposition temperature, took some time to reach equilibrium. In addition, the bed pressure drop was unknown at the start of each test series.

Accordingly, a simple bang-bang gas pressure control system was developed that allowed the operator to select a specific propellant delivery pressure. The instantaneous propellant tank pressure depended on both the ullage in the HTP tank and a potentiometer setting; the latter could be controlled by the operator and fixed the demanded tank pressure within the pressure control system. The initial aim was to achieve pseudo steady-state at a peroxide mass flow rate slightly higher than the design value of 17.7 g/s. Once this was achieved, by monitoring the flow meter turbine frequency, the demanded pressure was decreased so that the mass flow rate would gradually reduce in a blow-down configuration. This cycle was then repeated until the end of the run. This ensured that there was at least one epoch in the data

series for which the indicated mass flow rate corresponded to the design value of 17.7 g/s.

In all cases, the thruster run was initiated with a series of pulses or 'blips' – a rapid, manual opening and closing of the propellant solenoid valve just upstream of the thruster to pre-heat the catalyst bed. The valve was open for typically less than half a second in each blip. Once the temperature at the catalyst mid-bed position exceeded 300 °C, the valve was left open until shortly before propellant depletion.

Before starting the run series the volumetric flow meter was calibrated using water at the correct mass flow rate. The load cell for measuring thrust was calibrated before commencing each run series. It was not possible to perform many runs for the same condition in order to arrive at a formal statement of uncertainty. This would have consumed large quantities of HTP and human resources. However, certain comments can be made concerning the uncertainty of the experiment data.

Differential inputs were used for all thermocouple measurements. The uncertainties for the instrumentation used were ± 0.75 % for the mass flow rate, ± 0.1 % FSO for thrust, ± 0.75 % for temperature and ± 0.25 % for pressure. After taking into account calibration errors, the uncertainty for thrust increases to ± 0.5 %. The claimed uncertainty for C^* is ± 2 %, using pressure and mass flow rate (equation 2), and ± 0.5 %, using the temperature method (equation 1). Note, however, that the latter takes no account of uncertainties in the ratio of specific heats. The latter was estimated to be 1.275 according to the NASA CEA code [34]. In addition, the C^* measurement based on temperature assumes that the same axial temperature prevails across the internal diameter of the bed. The temperature near the wall is likely to be somewhat lower although the oxidation colouration observed on the outer

wall of the catalyst bed chamber and nozzle plenum suggests that the wall was indeed in excess of 500 °C. Consequently, it is estimated that the asymptotic (steady-state), temperature-based *C** data are likely to have an uncertainty of approximately ± 1.5 %.

3. Results and Discussion

3.1 Computational Fluid Dynamic Results

A typical output from the CFD model is shown in Figure 5, which illustrates the typical reduction in pressure across the bed. It was observed that the pressure drop was larger for lattice structures that were more dense. On the other hand, the average velocity of the flow reduces as the substrate structure becomes more complex and the flow path becomes more tortuous. Both observations were as expected.

A summary of the CFD model results for each of the four lattice designs is shown in Table 2. The 'density' is the ratio of solid volume to total volume. The table quite clearly shows the trade-off between the density (and hence surface area) and pressure drop. Designs 3 and 4, both lattice-based designs that have a complex structure, were considered the best, having the highest surface areas and acceptable pressure drops. As described earlier, to evaluate the relative performance of the two designs, a down-selection test strategy was devised that would allow simple evaluation tests to be carried out quickly on relatively small test samples, rather than the full-scale catalyst beds. In addition to the lattice design, other variables such as active phase coating procedure, lattice dimensions, etc. could be investigated. Then, once the most promising designs and coating strategies

were identified, full-scale catalyst bed manufacture was undertaken and these beds were then tested in the 20 N thruster.

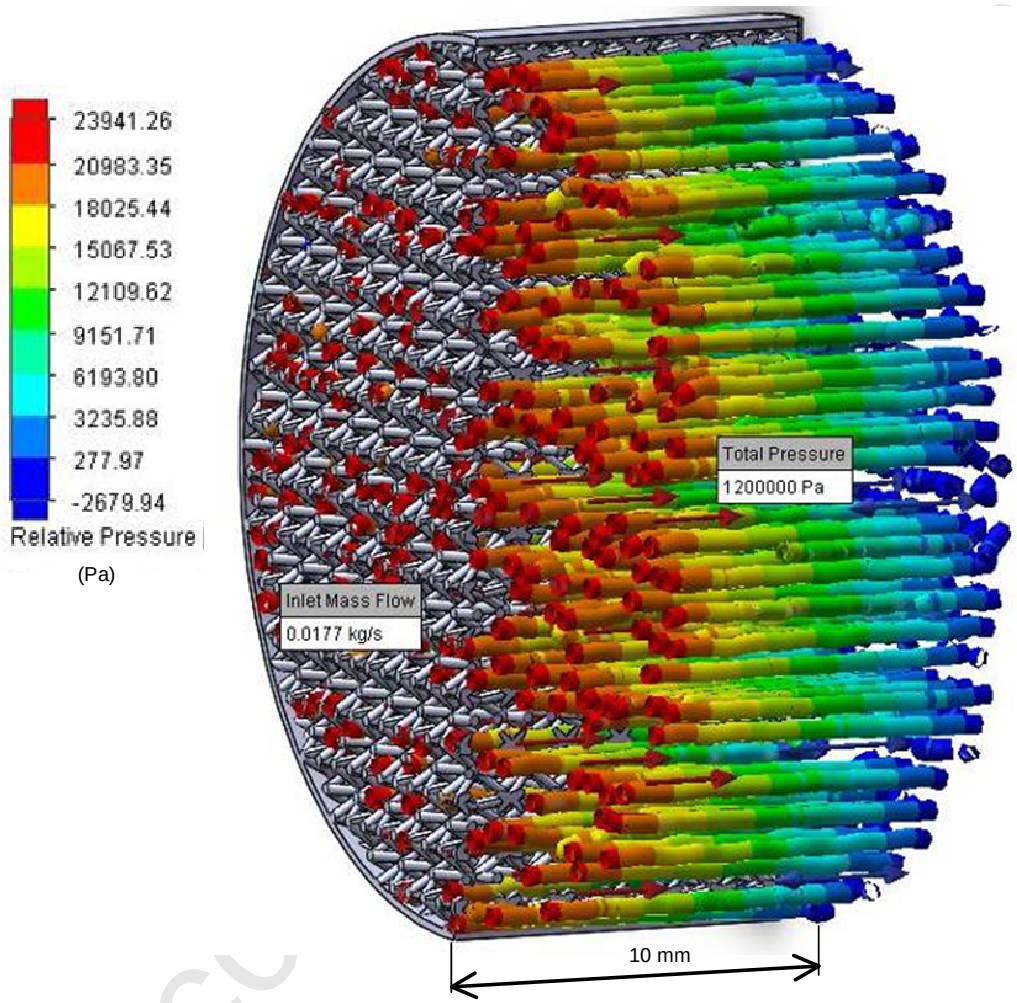

Figure 5: Typical CFD model output (Pressure drop across the catalyst bed segment)

Table 2: Summary of CFD model outputs

Model	Design 1	Design 2	Design 3	Design 4
Density %	6%	21%	26%	28%
Surface area/volume (mm^2/mm^3)	0.9	3	3.9	4.5
Pressure drop (Pa/mm)	313	1425	1940	3131

3.2 Down-selection of samples

As described earlier, drop tests were carried out on 15 samples with different geometries and wash coats (including the inert sample 0, see Table 1). In almost all cases, the reaction with the AM samples appeared to be more vigorous than with the MnO_x-coated ceria pellets used as the baseline comparator, although this was at least in part due to the difference in sample size, and hence surface area. In some cases, the AM samples were observed to fragment during exposure to the HTP. Although qualitative, the drop tests enabled a down-selection of 8 samples that showed good reactivity and had survived the drop tests without fragmenting. These samples were then subjected to the repeated immersion, dynamic weighing tests.

A result from one of these latter tests is shown in Figure 6. This is an example of a sample (sample 13A in Table 1) that did not perform particularly well, since even in the first immersion (Run 1), the rate of mass loss and rate of temperature rise was relatively low compared with some of the other samples, and the rates decreased significantly after each repeated immersion in HTP. To enable a comparison and ranking of the performance of each sample the following time parameters were determined from the test results:

a) Time to 60% mass loss (Run 1)
b) Time to 60% mass loss (Run 5)
c) Time to peak temperature (Run 1)
d) Time to peak temperature (Run 5)

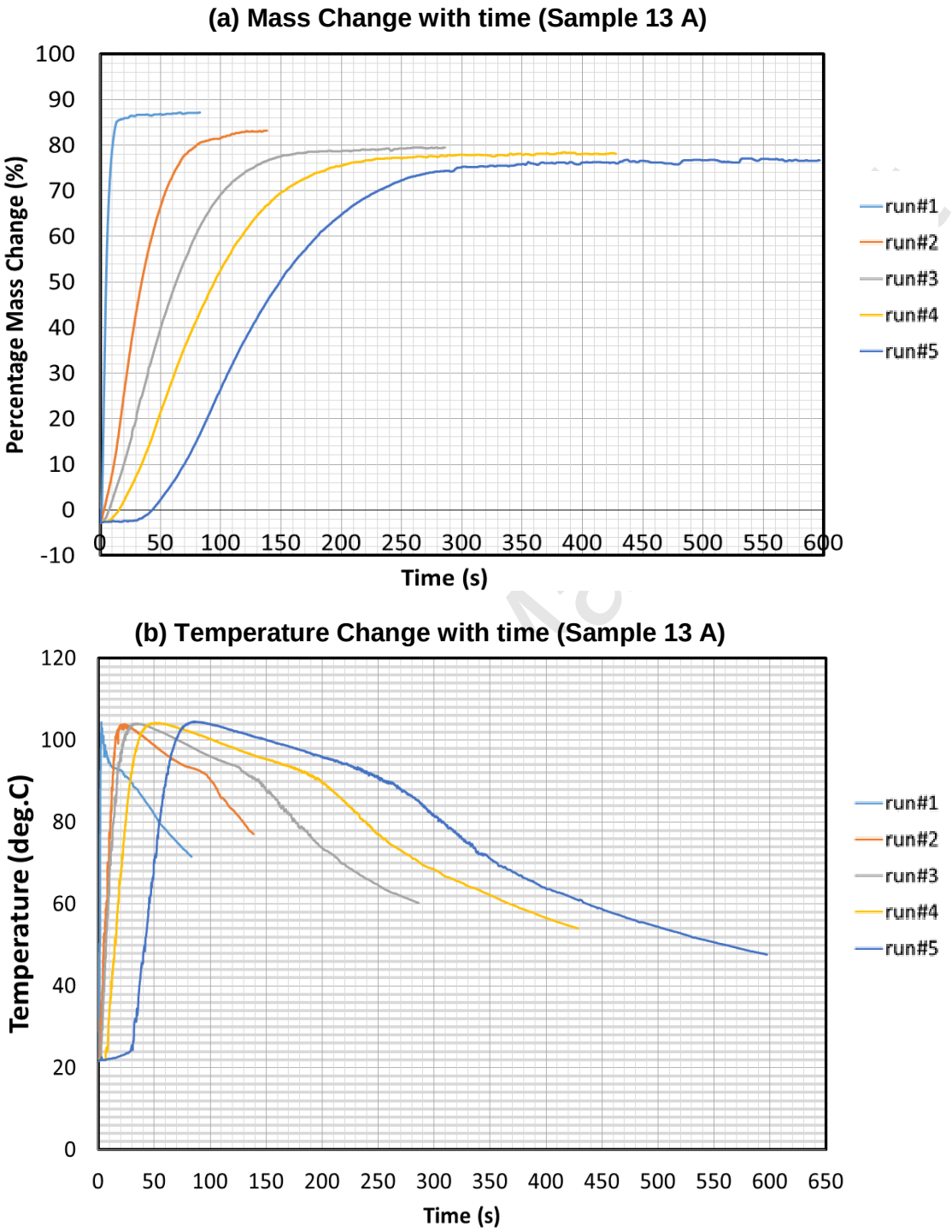

Figure 6: Typical sample screening test results

From the relative rankings derived from this initial series of dynamic weighing tests it became clear that the more dense (higher surface area) lattice designs (3 and 4)

were the more reactive and two of the samples (samples 5A and 12A, with washcoats of, respectively, gamma alumina plus carbon nanotubes and gamma alumina alone) were considered to be the most promising. A second batch of test samples was manufactured for further evaluation. A “design of experiments” (DOE) strategy was used to develop an experimental plan for testing the new batch of samples. Three parameters were included, where each parameter had two levels: these were lattice design (designs 3 and 4 described above), strut diameters (0.16 and 0.30 mm) and coatings (5A and 12A). In total, therefore, there were 8 variations to be tested.

After again carrying out qualitative drop tests with 87.5 % HTP (during which, encouragingly, none of the samples fragmented) a further series of dynamic weighing tests was performed. The initial reactivity of all of these samples was high and so the sample rankings were based on measurements of the time to 60% mass loss ($t_{60\%}$) and the time to peak temperature (t_{pT}) at the end of run 5. The results of these tests are summarised in Table 3:

Table 3: Summary of the dynamic weighing results

Experiment	Design	Strut diameter (mm)	Coating	$t_{60\%}$ (s)	t_{pT} (s)
1	3	0.16	5A	59.4	27.0
2	4	0.16	5A	40.4	26.4
3	3	0.30	5A	35.6	10.0
4	4	0.30	5A	8.7	4.1
5	3	0.16	12A	71.2	26.9
6	4	0.16	12A	161.4	40.2
7	3	0.30	12A	7.9	4.4
8	4	0.30	12A	19.7	7.1

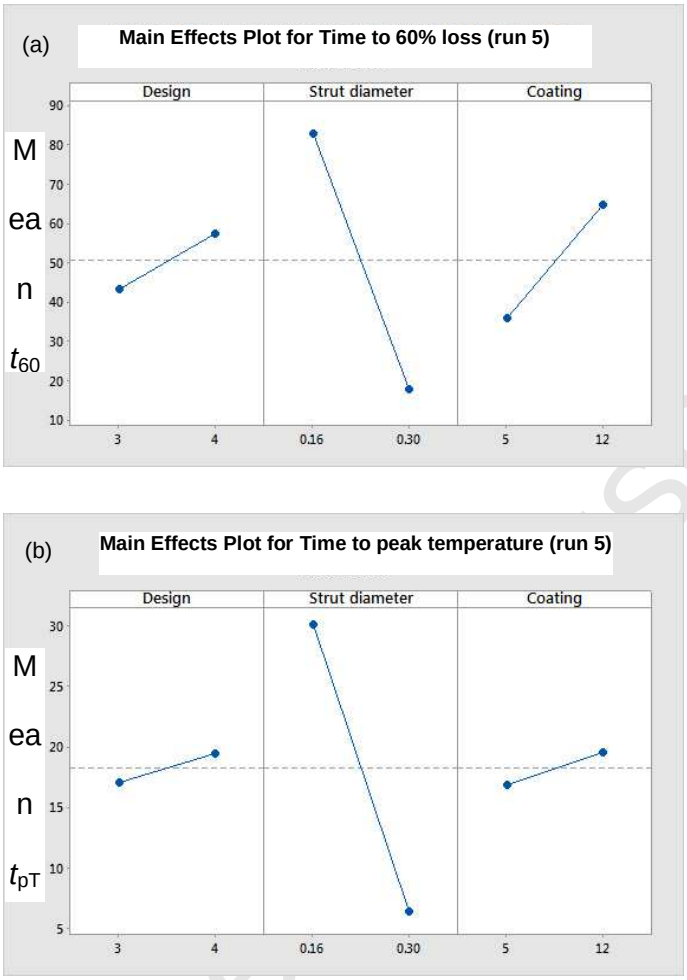

Figure 7: Results of DOE analysis (a) Time to 60% mass loss (b) Time to peak temperature.

After carrying out the DOE analysis it became clear that the strut diameter had the strongest influence on the results, with the larger diameter (0.3 mm) being the better in terms of relative reactivity, whereas the influence of lattice design and type of coating was less strong, see Figure 7. As a result of these down-selection tests on the catalyst samples, it was decided to manufacture and test full-scale catalyst beds based on designs 3 and 4, with lattice strut diameters of 0.3 mm and with coatings 5A and 12A. These beds were designated 3.5A, 4.5A, 3.12A and 4.12A (the “A” designating alumina as the substrate material). Figure 8 shows one of the full-scale

catalyst bed inserts (two per bed) before coating with the active phase (left) and afterwards (right).

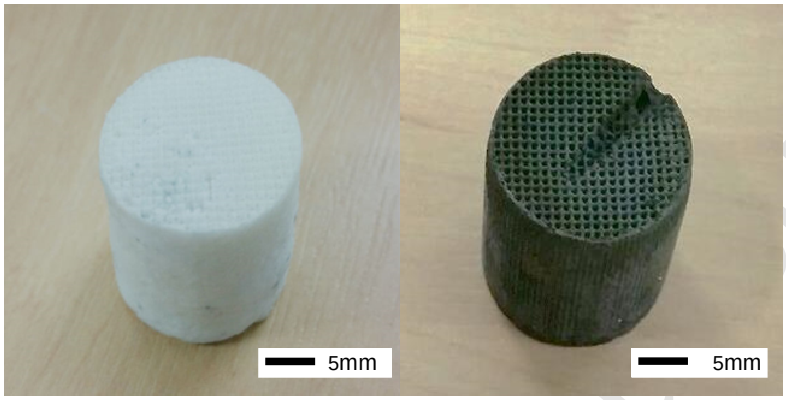

Figure 8: Full-scale catalyst bed inserts before (left) and after coating with the active phase (right). The groove allows for the fitting of a thermocouple.

Figure 9 and Figure 10, show, respectively, SEM images of the full-scale bed designs 3 and 4 (a) before and (b) after coating with the active phase/wash coat number 5. In each case a small region has been selected for energy dispersive X-ray spectroscopic (EDS) analysis. It is seen that the coatings reduce the void fraction but increase the effective surface area exposed to the HTP. Specific surface area (SSA) measurements before and after coating confirmed this observation: the BET surface area of all the samples before coating was below 1 m^2/g whereas it was increased to 18.3 m^2/g, 5.6 m^2/g, 38.4 m^2/g, 24.3 m^2/g after coating for samples 3.5A, 3.12A, 4.5A, and 4.12A, respectively. The increase in surface area is desirable to promote HTP decomposition but the reduction in void fraction will cause an increase the pressure drop across the catalyst bed. The EDS data confirm that the un-coated lattice structures predominantly comprise aluminium and oxygen (alumina), with traces of silicon and magnesium from the feedstock powder used to create the AM structures. The oxygen content percentage indicates a good oxidation process and is in

agreement with the presence of Al_2O_3, SiO_2 and MgO. The EDS data obtained from the surface of the coated samples confirms the predominant presence of manganese, oxygen, and sodium (from the sodium permanganate solution used to form the active phase layer). The negligible amount of aluminium indicates a good coating process. On the other hand, the sodium to manganese percentage is close to one, thus showing that all the sodium remains on the surface; moreover, the surface amount of oxygen displays clearly that the average oxidation number of manganese is in agreement with the possible formation of Na_xMnO_2.

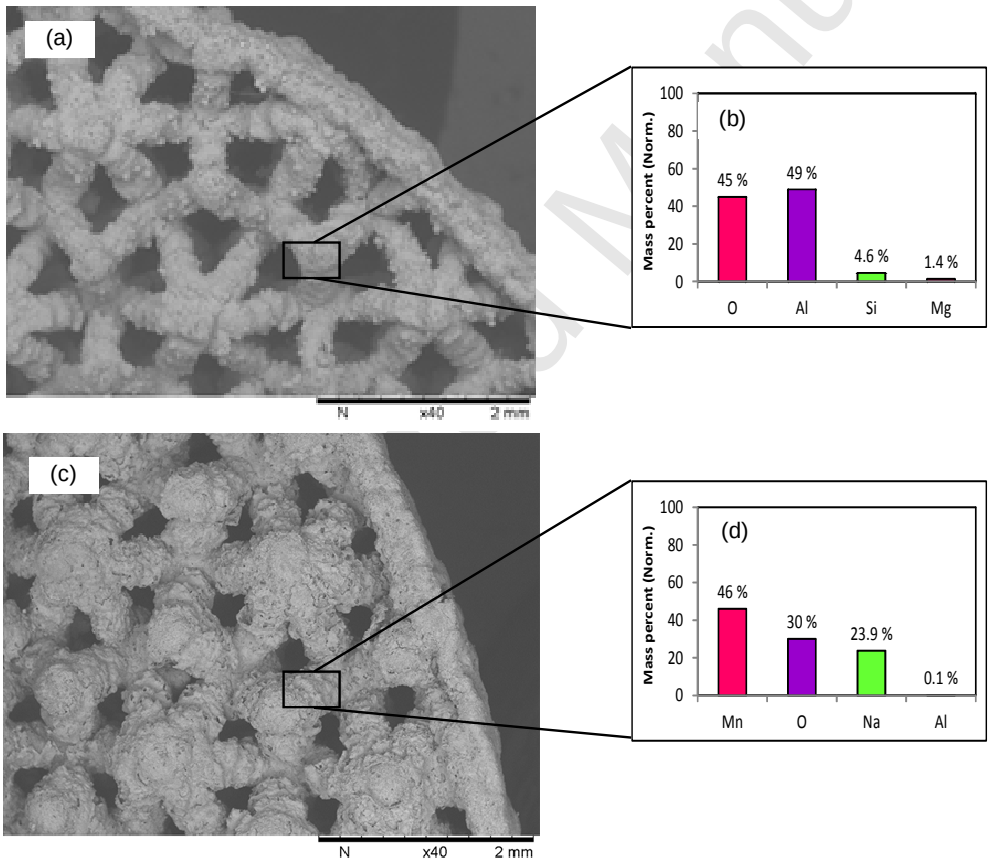

Figure 9: (a) SEM image of design 3 before coating (b) EDS chemical analysis of design 3 before coating (c) SEM image of design 3 after coating with the active phase/washcoat #5 (d) EDS chemical analysis of design 3 after coating.

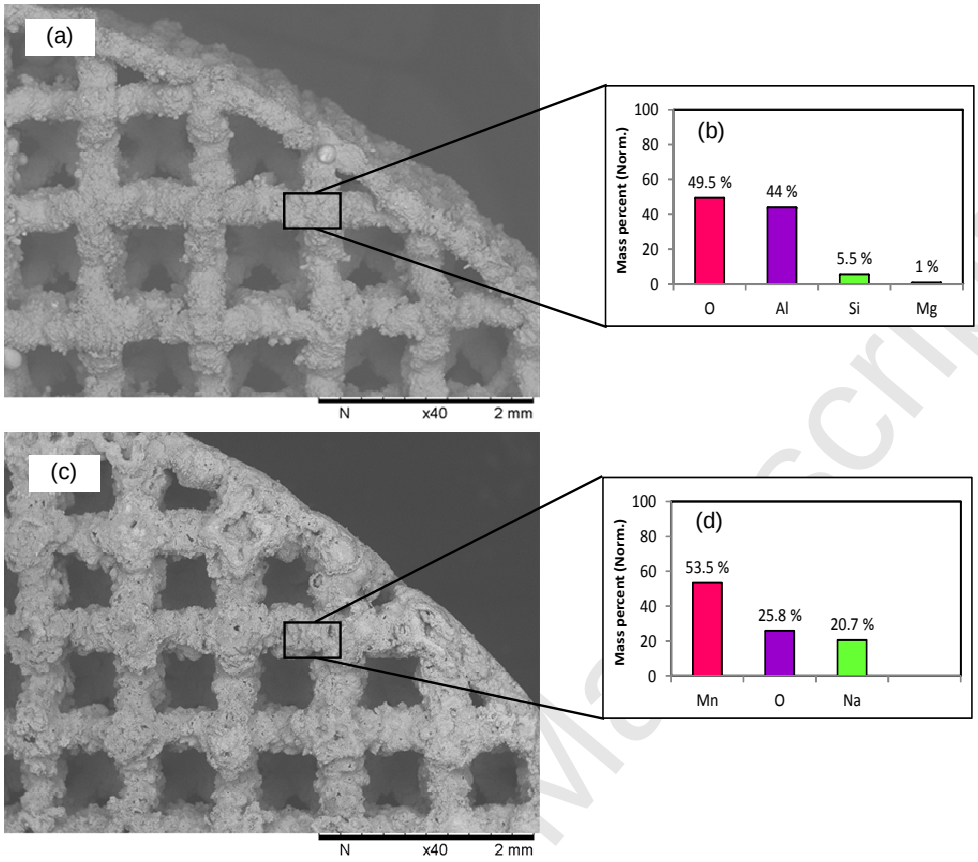

Figure 10: a) SEM image of design 4 before coating (b) EDS chemical analysis of design 4 before coating (c) SEM image of design 4 after coating with the active phase/washcoat #5 (d) EDS chemical analysis of design 4 after coating.

3.3 Thruster Tests

This section presents a summary of the results of the thruster tests. Of particular interest are the decomposition temperature (since this drives *C**), thrust, sea-level specific impulse, the start-up characteristics and any evidence of exhaustion of the active phase.

It is important to note that the HTP liquid undergoes several stages of decomposition. At some distance downstream of the injector plate, the peroxide decomposes into three gases: oxygen, steam and peroxide vapour (the last

decomposes thermally and chemically rather rapidly). Upstream of this position, or phase-change plane, the fluid is in two phases, liquid and gas. It is a matter of conjecture as to the most desirable position of this phase-change plane. Since the gas phase produces a much higher pressure-drop, on account of the speed of advancement through the bed, it is desirable to shorten the length within the bed occupied by gas. On the other hand, if the fluid becomes completely gaseous a short distance from the injector then it is likely that the bed will have a longer life.

When testing bed 3.12A, clouds of steam were seen coming from the nozzle in such quantities that they overwhelmed the laboratory's exhaust-ducting system. Further testing of this bed was abandoned because it was deemed unsafe to proceed further. Beds 3.5A and 4.5A showed premature signs of active phase exhaustion after an HTP throughput of about 1 kg, although both exhibited a C^* efficiency > 99 % based on temperature in the early phase of the runs. Accordingly, this paper focuses on the results for the more promising bed 4.12A, the results for which are presented in Figures 11 – 14. It should be noted that in all the beds tested there was very little sign of mechanical attrition or cracking.

Figure 11 shows the temperature histories for the thermocouple readings at both the mid-point position of the bed and the nozzle's plenum chamber. The first heating pulse occurred at approximately time t = 23.3 s; the second rise in temperature (at approximately t = 27.4 s) occurred when the operator commanded the propellant solenoid valve to open fully. For both events, there is no significant lag between the temperature rise recorded at the mid-point position and that recorded in the nozzle plenum chamber. However, due to the combined effects of thermal inertia and heat losses the nozzle plenum temperature takes longer to reach equilibrium than the mid-point temperature. This was also observed in the baseline runs with the MnOx-

coated ceria pellets. As noted earlier, the thruster design had not been optimised from a thermomechanical point of view and so its thermal mass and heat losses were higher than would be expected in a flight-rated thruster. In the case of the mid-point thermocouple, the temperature record shows values that are above the theoretical maximum temperature for the adiabatic decomposition of 87.5 % HTP (approximately 695 °C) and therefore must be regarded with suspicion. The catalyst shows good reactivity after a single starting pulse; this should be compared with the 6 pulses needed for the baseline MnOx-coated ceria pellets to achieve a temperature in excess of 300 °C mid-way along the bed.

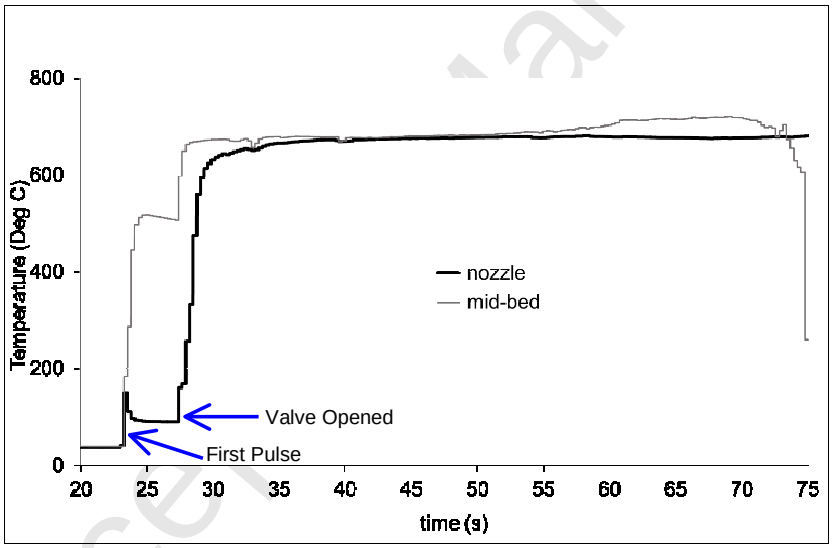

Figure 11: Catalyst bed 4.12A temperature history

Figure 12 shows the indicated mass flow rate during the pseudo steady-state part of the run, from 45 s to 75 s. The trace reflects the operator's use of the potentiometer, with the propellant feed pressure being ramped up during the time interval 45 – 52 s before allowing the system to settle in blow-down mode from 52 – 70 s. The "stepping" in the signal is due to signal averaging over 0.5s intervals to determine accurately the turbine frequency and hence HTP flow rate. It can be seen that the

flow rate matches the target value of 17.7 g/s on four occasions and that it appears to be maintained just before the end of the run.

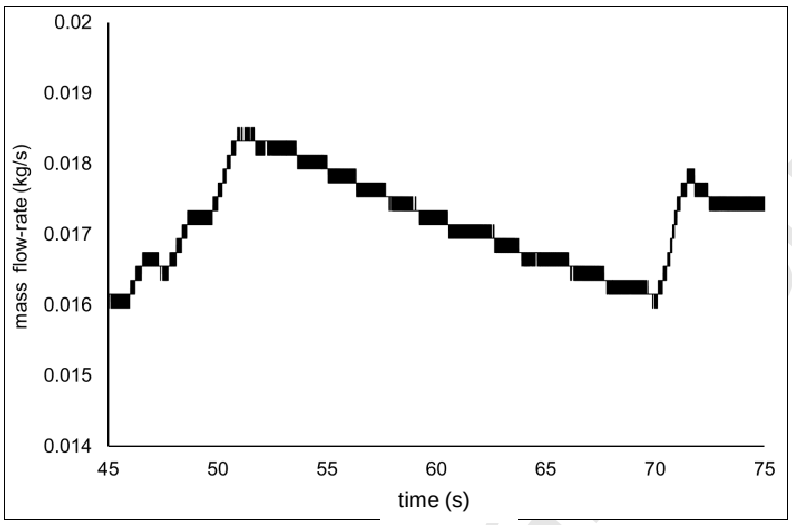

Figure 12: Catalyst bed 4.12A mass flow rate

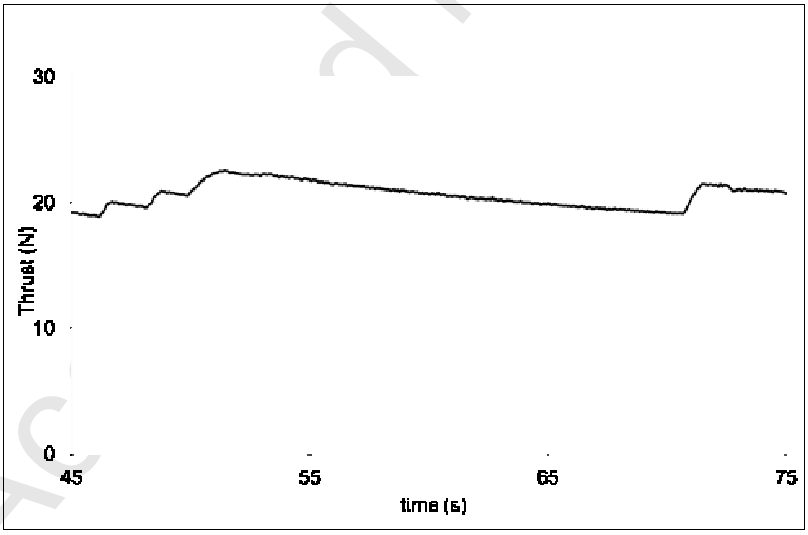

Figure 13: Thrust history with catalyst bed 4.12A

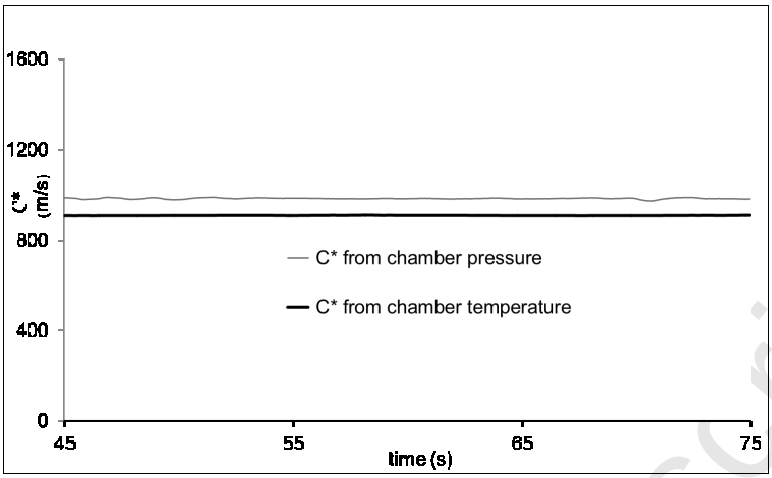

Figure 14: Catalyst bed 4.12A *C** history

Figure 13 shows the thrust history recorded during this same time interval: it is observed that the variation in thrust closely matches that of the propellant mass flow rate.

Figure 14 shows the instantaneous values of *C**, calculated using a 60-second rolling average. The *C** based on pressure and mass flow rate (equation 2) is clearly in error since it is significantly higher than the theoretical value of 909 m/s. This suggests a failure in the nozzle plenum pressure transducer. Unfortunately, there were insufficient HTP resources available to repeat this run with a replacement unit. The *C** based on temperature (equation 1) leads to a *C** efficiency of 100±1.5 % based on an HTP concentration of 87.5 %. Note that the concentration of HTP has an uncertainty of ±1.0 % so it is likely that the actual concentration used was slightly higher than 87.5 %.

A summary of the results for catalyst bed 4.12A is compared with that of the baseline MnOx-coated ceria pellets in Table 4.

Table 4: Comparison between Bed 4.12A and the Baseline Ceria Pellets

Parameter	Baseline	4.12A
*C** (m/s) (from temperature data)	886±18	909±14
*C** efficiency (%)	97.5±2	100±1.5
Thrust (N)	17.5±0.08	21.2±0.1
Sea level specific impulse (s)	101±1.2	122±1.4
Pressure drop (bar) (including retainer plate)	3.1±0.016	3.2±0.016

The AM bed out-performed the baseline pellets in terms of *C** efficiency, when estimated using the temperature data. Bed 4.12A achieved a sea-level specific impulse of 122 s, at the design HTP mass flow rate, which is significantly higher than the baseline value. Surprisingly, the pressure drop for bed 4.12.A is almost the same as for the baseline ceria bed; it must be remembered though that although the AM-bed is loosely described as being monolithic, in fact the internal topography is deliberately convoluted.

Overall, it is difficult to draw a conclusion as to whether or not the AM-manufactured bed 4.12A is superior to the baseline ceria catalyst. This is because of the lack of information concerning lifetime. The baseline catalyst has a heritage at the University of Southampton that indicates a much higher peroxide throughput can be endured than the 2.25 kg to which bed 4.12A was exposed in the present tests. Nevertheless, the *C** performance is very encouraging and suggests further testing and development is needed.

4. CONCLUSIONS

This paper has described the development of novel and high performance monolithic catalyst beds for the use in a hydrogen peroxide (HTP) monopropellant thruster using the robustness of additive manufacturing. The design strategy introduced here is based on designing a flow-controlled catalyst bed. It was found that a nodal diamond-shape lattice design satisfies the requirements of AM overhanging structures and therefore different configurations of nodal diamond-shape based catalyst beds were studied. From the computational fluid dynamic results, it was found that catalyst beds with lattice struts arranged in hexagonal shape and lattices arranged with one layer of lattice structure rotated by 90 ° from the previous layer show the highest geometrical surface area and acceptable pressure drop. The two designs were successfully manufactured using alumina, derived from aluminium-silicon-magnesium powder that was laid down by selective laser melting, as the substrate material with a strut thickness of 0.15 – 0.30 mm. Each design was coated with gamma alumina and a mixture of gamma alumina and carbon nanotubes (CNT), followed by coating with an active phase of oxides of manganese (MnOx) derived from a solution of sodium permanganate.

Of the four full-scale beds that were produced, three exhibited good performance initially, although the performance of two of these beds later showed signs of deterioration after only a modest throughput of HTP had been achieved. The best-performing AM catalyst bed remained fully active throughout the testing and exhibited better performance results than the same bed chamber containing MnOx-coated ceria pellets, used as a baseline comparator a C^* of 909 m/s, C^* efficiency of 100 %, thrust of 21.2 N and sea level specific impulse of 122 s. The bed pressure drop was approximately the same as the baseline comparator with a value of 3.2 bar.

This is therefore considered to be a very promising development and an appropriate application of AM technology.

The work carried out in this research is forecasted to have particular impacts on the catalytic and aerospace industries in different aspects such as:

a. Design innovation of the catalyst beds.
b. Less material waste, production cost and reduced time to market with the use of AM.
c. Thruster compactness and performance
d. Environmental and safety procedures via the use of green monopropellant

5. Acknowledgements

This work was supported by the European Space Agency following a contract let in response to the Invitation to Tender (ITT) number 7510, dated May 2013. The authors wish to acknowledge the support of Céramiques Techniques Industrielles, France, by providing the ceria pellets from which the baseline comparator catalyst was fabricated. .

6. REFERENCES

[1] B. Ritz, Y. Zhao, A. Krishnadasan, N. Kennedy, H. Morgenstern, Estimated effects of hydrazine exposure on cancer incidence and mortality in aerospace workers, Epidemiology, 17 (2006) 154-161.

[2] H.K. Ciezki, K.W. Naumann, Some Aspects on Safety and Environmental Impact of the German Green Gel Propulsion Technology, Propellants, Explosives, Pyrotechnics, 41 (2016) 539-547.

[3] G. Pace, A. Pasini, L. Torre, "Test bench for the unsteady characterization of a pulsed green monopropellant thruster," in *51st AIAA/SAE/ASEE Joint Propulsion Conference*, 2015, pp. 1-16.

[4] A.S. Gohardani, J. Stanojev, A. Demairé, K. Anflo, M. Persson, N. Wingborg, C. Nilsson, Green space propulsion: Opportunities and prospects, Progress in Aerospace Sciences, 71 (2014) 128-149.

[5] A. Asghar, A.A.A. Raman, W.M.A.W. Daud, Advanced oxidation processes for in-situ production of hydrogen peroxide/hydroxyl radical for textile wastewater treatment: A review, Journal of Cleaner Production, 87 (2015) 826-838.

[6] V. Touch, S. Hayakawa, S. Yamada, S. Kaneko, Effects of a lactoperoxidase-thiocyanate-hydrogen peroxide system on Salmonella enteritidis in animal or vegetable foods, International Journal of Food Microbiology, 93 (2004) 175-183.

[7] S. Jo, D. Jang, J. Kim, H. Yoon, S. Kwon, "Chugging instability of H2O2 monopropellant thrusters with catalyst reactivity and support sizes," in *47th AIAA/ASME/SAE/ASEE Joint Propulsion Conference and Exhibit 2011*, 2011, pp. 920-924.

[8] A. Pasini, L. Torre, L. Romeo, L. D'Agostino, "Performance modeling and analysis of H2O2 catalytic pellet reactors," in *44th AIAA/ASME/SAE/ASEE Joint Propulsion Conference and Exhibit*, 2008, pp. 1-15.

[9] Y. Batonneau, R. Brahmi, B. Cartoixa, K. Farhat, C. Kappenstein, S. Keav, G. Kharchafi-Farhat, L. Pirault-Roy, M. Saouabé, C. Scharlemann, Green Propulsion: Catalysts for the European FP7 Project GRASP, Topics in Catalysis, 57 (2014) 656-667.

[10] A. Cervone, L. Torre, A. Pasini, L. Romeo, L. D'Agostino, "Development of hydrogen peroxide rockets at alta S.P.A.: The past, the present and the future," in *Proceedings of the International Astronautical Congress, IAC*, 2012, pp. 7491-7501.

[11] L. Torre, L. Romeo, A. Pasini, A. Cervone, L. d'Agostino, "Propulsive performance of a 100 μm Pt/CexZr1-x/Al2O3 catalytic bed," in *47th AIAA/ASME/SAE/ASEE Joint Propulsion Conference and Exhibit 2011*, 2011, pp. 1-12.

[12] A. Adami, M. Mortazavi, M. Nosratollahi, M. Taheri, J. Sajadi, Multidisciplinary Design Optimization and Analysis of Hydrazine Monopropellant Propulsion System, International Journal of Aerospace Engineering, 2015 (2015) 9.

[13] H. Tian, T. Zhang, X. Sun, D. Liang, L. Lin, Performance and deactivation of Ir/γ-Al2O3 catalyst in the hydrogen peroxide monopropellant thruster, Applied Catalysis A: General, 210 (2001) 55-62.

[14] J. Bejhed, J. Wallbank, R. Lindegren, R. Thorslund, A.M. Baker, L. Stenmark, J. Köhler, Catalyst microsystem design and manufacture for a monopropellant microrocket engine, PowerMEMS Kyoto, Japan, 2004.

[15] O. Božić, D. Porrmann, D. Lancelle, S. May, Enhanced development of a catalyst chamber for the decomposition of up to 1.0 kg/s hydrogen peroxide, CEAS Space Journal, 8 (2016) 77-88.

[16] M.J. Palmer, G.T. Roberts, A.J. Musker, "Design, build and test of a 20N hydrogen peroxide monopropellant thruster," in *47th AIAA/ASME/SAE/ASEE Joint Propulsion Conference and Exhibit 2011*, 2011, pp. 1-17.

[17] Bramanti C., Musker J., Place W., Solent L, Experimental Characterization of Advanced Materials for the Catalytic Decomposition of Hydrogen Peroxide, 42nd AIAA/ASME/SAE/ASEE Joint Propulsion Conference & Exhibit, American Institute of Aeronautics and Astronautics2006, pp. 1-12.

[18] A. Uriondo, M. Esperon-Miguez, S. Perinpanayagam, The present and future of additive manufacturing in the aerospace sector: A review of important aspects, Proceedings of the Institution of Mechanical Engineers, Part G: Journal of Aerospace Engineering, 229 (2015) 2132-2147.

[19] A. Sabouri, A.K. Yetisen, R. Sadigzade, H. Hassanin, K. Essa, H. Butt, Three-Dimensional Microstructured Lattices for Oil Sensing, Energy & Fuels, (2017).

[20] H. Hassanin, F. Modica, M. El-Sayed, J. Liu, K. Essa, Manufacturing of Ti-6Al-4V Micro-Implantable Parts using Hybrid Selective Laser Melting and Micro-electrical Discharge Machining, Advanced Engineering Materials, (2016).

[21] L.N. Carter, K. Essa, M.M. Attallah, Optimisation of selective laser melting for a high temperature Ni-superalloy, Rapid Prototyping Journal, 21 (2015) 423-432.

[22] M.J. Palmer, G.T. Roberts, A.J. Musker, Manufacture, Assessment and Down-Selection of Catalysts for the Decomposition of Hydrogen Peroxide, paper presented at European conference for aerospace sciences (eucass)Saint Petersburg, Russia, 2011.

[23] M. Palmer, G. Roberts, A. Musker, Design, Build and Test of a 20 N Hydrogen Peroxide Monopropellant Thruster, 47th AIAA/ASME/SAE/ASEE Joint Propulsion Conference & Exhibit, American Institute of Aeronautics and Astronautics2011, pp. 1-17.

[24] M.J. Palmer, G.T. Roberts, A.J. Musker, "Design, build and test of a 20N hydrogen peroxide monopropellant thruster," in *47th AIAA/ASME/SAE/ASEE Joint Propulsion Conference and Exhibit 2011*, 2011.

[25] G.T. Roberts, A.J. Musker, D. Beechey, N. El-Batal, B. Profir, N. Spencer, N. Tenev, M. Wills, Development of a small-scale hybrid thruster using hydrogen peroxide as the oxidiser, paper 2981545 presented at Space Propulsion 2014 Cologne, Germany, 2014.

[26] P. Colombo, H.P. Degischer, Highly porous metals and ceramics, Materials Science and Technology, 26 (2010) 1145-1158.

[27] D. Manfredi, F. Calignano, E.P. Ambrosio, M. Krishnan, R. Canali, S. Biamino, M. Pavese, E. Atzeni, L. Luliano, P. Fino, C. Badini, Direct Metal Laser Sintering: An additive manufacturing technology ready to produce lightweight structural parts for robotic applications, Metallurgia Italiana, 105 (2013) 15-24.

[28] L.E. Murr, S.M. Gaytan, F. Medina, M.I. Lopez, E. Martinez, R.B. Wicker, "Additive layered manufacturing of reticulated Ti-6Al-4V biomedical mesh structures by electron beam melting," in *IFMBE Proceedings*, 2009, pp. 23-28.

[29] C. Qiu, S. Yue, N.J.E. Adkins, M. Ward, H. Hassanin, P.D. Lee, P.J. Withers, M.M. Attallah, Influence of processing conditions on strut structure and compressive properties of cellular lattice structures fabricated by selective laser melting, Materials Science and Engineering A, 628 (2015) 188-197.

[30] S. Li, H. Hassanin, M.M. Attallah, N.J.E. Adkins, K. Essa, The development of TiNi-based negative Poisson's ratio structure using selective laser melting, Acta Materialia, 105 (2016) 75-83.

[31] J. Brennan-Craddock, D. Brackett, R. Wildman, R. Hague, The design of impact absorbing structures for additive manufacture, Journal of Physics: Conference Series, 382 (2012) 012042.

[32] D.J. Jarvis, W.E. Voice, N.J.E. Adkins, H. Hassanin, "Manufacturing of a ceramic article from a metal preform or metal matrix composite preform provided by 3d-printing or 3d-weaving," USA Patent WO2015081996 A1, 2015.

[33] P. Surmacz, Influence of various types of Al_2O_3/Mn_xO_y catalysts on performance of a 100 mm chamber for decomposition of 98 %+ hydrogen peroxide, Transactions of the institute of aviation, 3 (2015) 58-68.

[34] S. Gordon, B.J. McBride, Computer Program for Calculation of Complex Chemical Equilibrium Compositions and Applications, NASA RP-1311, (1994).

Additively Manufactured Monolithic Catalyst Bed for HTP Thruster Applications

K. Essa[(1)], H. Hassanin[(2,3)], M.M. Attallah[(3)], N.J. Adkins[(3)], A.J. Musker[(4)], G.T. Roberts[(5)], N.Tenev[(5)], M. Smith[(6)]

[(1)]School of Mechanical Engineering, University of Birmingham, UK, Email: k.e.a.essa@bham.ac.uk
[(2)]School of Mechanical and Automotive Engineering, Kingston University; Formerly, School of Metallurgy & Materials, University of Birmingham, UK., Email: h.hassanin@kingston.ac.uk
[(3)] School of Metallurgy & Materials, University of Birmingham, UK.
[(4)]DELTACAT Ltd and University of Southampton, UK, Email: tony.musker@deltacatuk.com
[(5)]Aerodynamics & Flight Mechanics Research Group, University of Southampton, UK, Email: gtr@soton.ac.uk
[(6)]TEC-MPC, ESA/ESTEC, NL, Email: Matthew.Smith@esa.int

Highlights

- A novel monolithic catalyst bed design methodology has been introduced aiming to have complex geometry and high geometrical surface area whilst achieving an acceptable pressure drop.
- Additive manufacturing has been successfully implemented as a novel technology to manufacture catalyst bed designs. Precision ceramic beds with minimum features of 150-300 micron have been obtained.
- The developed AM catalyst beds show a C* of 909 m/s, C* efficiency of 100%), thrust of 21.2 N, sea level impulse of 122 and pressure drop of 3.2 bar.
- The AM monolithic catalyst beds developed in this research show high performance in many aspects when compared to the baseline ceria pellets catalyst beds.